Review of Scientific Instruments

RESEARCH ARTICLE | OCTOBER 12 2023

An ultra-low field SQUID magnetometer for measuring antiferromagnetic and weakly remanent magnetic materials at low temperatures

Michael Paulsen; Julian Lindner; Bastian Klemke; Jörn Beyer; Michael Fechner; Dennis Meier; Klaus Kiefer

Rev. Sci. Instrum. 94, 103904 (2023)
https://doi.org/10.1063/5.0135877

AIP Publishing

Review of Scientific Instruments | ARTICLE | pubs.aip.org/aip/rsi

An ultra-low field SQUID magnetometer for measuring antiferromagnetic and weakly remanent magnetic materials at low temperatures

Cite as: Rev. Sci. Instrum. 94, 103904 (2023); doi: 10.1063/5.0135877
Submitted: 23 November 2022 • Accepted: 25 September 2023 •
Published Online: 12 October 2023

View Online Export Citation CrossMark

Michael Paulsen,[1,a)] Julian Lindner,[2] Bastian Klemke,[2] Jörn Beyer,[1] Michael Fechner,[3] Dennis Meier,[4,5] and Klaus Kiefer[2]

AFFILIATIONS

[1] Physikalisch-Technische Bundesanstalt Berlin (PTB), 7.6 Cryosensors, Abbestrasse 2-12, 10587 Berlin, Germany
[2] Helmholtz-Zentrum Berlin für Materialien und Energie (HZB), Sample Environment Group, Hahn-Meitner-Platz 1, 14109 Berlin, Germany
[3] Max Planck Institute for the Structure and Dynamics of Matter, Luruper Chaussee 149, 22761 Hamburg, Germany
[4] Norwegian University of Science and Technology (NTNU), Department of Materials Science and Engineering, Sem Sælandsvei 12, N-7034 Trondheim, Norway
[5] Center for Quantum Spintronics, Department of Physics, NTNU, Trondheim 7491, Norway

[a)] Author to whom correspondence should be addressed: michael.paulsen@ptb.de

ABSTRACT

A novel setup for measuring magnetic fields of antiferromagnets (i.e., quadrupolar or higher-order magnetic fields) and generally weakly remanent magnetic materials is presented. The setup features a highly sensitive superconducting quantum interference device magnetometer with a magnetic field resolution of ~ 10 fT and non-electric temperature control of the sample space for a temperature range of 1.5–65 K with a non-electric sample movement drive and optical position encoding. To minimize magnetic susceptibility effects, the setup components are degaussed and realized with plastic materials in sample proximity. Running the setup in magnetically shielded rooms allows for a well-defined ultra-low magnetic background field well below 150 nT *in situ*. The setup enables studies of inherently weak magnetic materials, which cannot be measured with high field susceptibility setups, optical methods, or neutron scattering techniques, giving new opportunities for the research on, e.g., spin-spiral multiferroics, skyrmion materials, and spin ices.

I. INTRODUCTION

The macroscopic magnetic field of a material is given by its susceptibility to the magnetic background field and, depending on the micromagnetic moments of the sample, its inherent magnetism. Conventional ferro-/ferrimagnets, such as iron, cobalt, and nickel compounds, exhibit pronounced magnetic fields > μT that can readily be measured by inductive coils or fluxgate devices. In contrast, the complex magnetic order of spin ice, spin-spiral multiferroics, skyrmions lattices, antiferromagnets, and other emergent functional materials is often hard to detect with characteristic magnetic field values as low as pT. Furthermore, depending on the material's susceptibility, it can be difficult to ensure non-invasive magnetization measurements and to probe the intrinsic magnetic properties free from interfering magnetic background contributions. Achieving such experimental conditions is challenging due to the earth magnetic field, remanence in experimental setup materials, and the currents of electronic devices, as depicted in Fig. 1.

The motivation for realizing an appropriate ultra-low-field variable temperature magnetometer was seminal magnetization measurements on antiferromagnets. Generally, antiferromagnets have been studied for several decades in fundamental research and, more recently, as materials of interest in spintronic

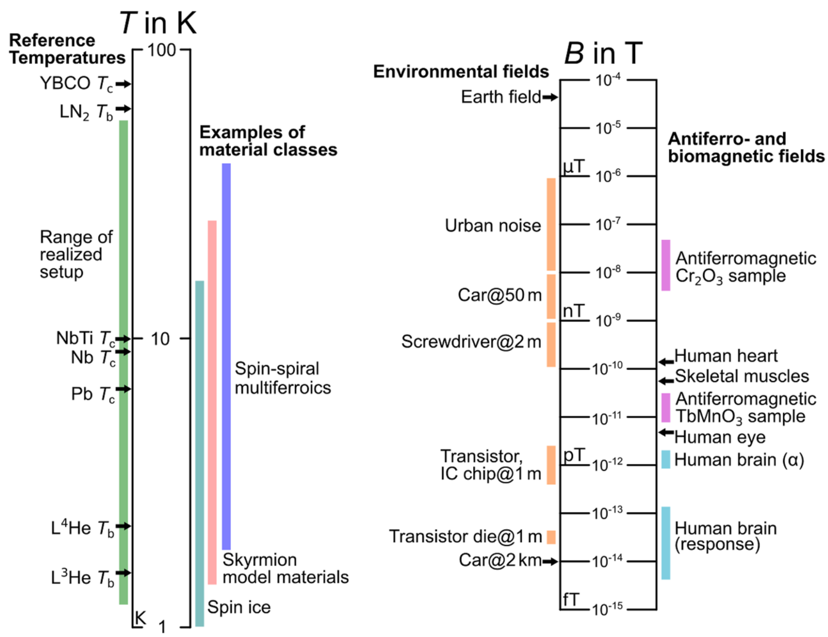

FIG. 1. Overview of temperatures[1] T_x (x = b [boiling], c [critical]), materials, and magnetic field strengths[2] that are relevant for the type of measurements addressed by the developed setup. Significant examples of material systems are spin-spiral multiferroics, such as orthorhombic rare-earth manganites[3,4] $RMnO_3$ (R = Gd, Tb, Dy), manganese tungstate[5] and the olivine[6] Mn_2GeO_4, classical skyrmion materials[7,8] (e.g., MnSi, $Fe_{1-x}Co_xSi$), and spin ice materials, such as the pyrochlore[9] $Dy_2Ti_2O_7$.

devices.[10] As there is no intrinsic, macroscopic dipole field in the antiferromagnetic phase, measuring this state usually involves sophisticated methods, e.g., neutron scattering facilities[11,12] or susceptibility setups involving high magnetic fields.[13] An instructive classical example of an antiferromagnetic solid state system with an ultra-weak intrinsic magnetic field is Cr_2O_3. It was predicted[14] to exhibit very weak, higher-order intrinsic, macroscopic magnetization (~ 10 nT for a single domain, spherical sample with radius ~ 3.2 mm). The few confirmed measurements of the respective quadrupolar magnetic fields were all conducted using dedicated Superconducting QUantum Interference Device (SQUID) setups, which are not commercially available.[15,16] Common to these setups is that the SQUID sensor and its superconducting pick-up coil need to be operated at an ideally constant low temperature [< 9 K (77 K) for low (high) temperature superconductors]. In addition, the pick-up coil needs to be close (≤ 15 mm) to the sample to cause a sufficiently strong magnetic signal. Since SQUID magnetometers detect magnetic flux *change*, the sample is typically moved relative to the pick-up coil. Furthermore, the magnetic background field must be kept extremely low to avoid magnetization of the sample due to its magnetic susceptibility. Notably, the magnetic shielding was not quantitatively described in the constant- and variable-temperature setups in the literature.[15–17] This is a crucial issue as unwanted magnetization may lead to false quadrupole-like signals in the case of anisotropic magnetic susceptibility. It should be noted that commercially available SQUID measurement systems typically involve electrical heaters and large magnets.[13] While these can nominally be degaussed down to zero field, it is not clear if the actual background field within such a setup is significantly below the necessary 1 Oe, i.e., 100 μT, to avoid false signals due to anisotropic susceptibility.[16] Furthermore, the gradiometric pick-up coil of commercial systems is usually optimized for measuring the magnetic dipole moment of the sample, rather than higher-order magnetic contributions. However, a recent state-of-the-art commercial SQUID setup offers sample rotation with magnetic background fields below 5 μT.[18]

The realization of a magnetometer with very low magnetic background and high magnetic field resolution has recently been described by the authors.[19] In that setup, the sample was kept at constant liquid helium temperature (T_{LHe} = 4.2 K) and slowly rotated using a plastic gravity-driven pendulum motor along with an optical encoder, ~ 4 mm in front of a superconducting pick-up coil connected to a SQUID sensor. The magnetometer can advantageously be used in combination with a Glass-Fiber-reinforced Cryostat (GFC) inside of a magnetically shielded environment, such as Berlin Magnetically Shielded Room-2 (BMSR-2)[20] or a smaller ultra-low magnetic field shielding.[21] Equipping the setup[19] with a temperature control of the sample is non-trivial as this may increase the magnetic background substantially due to electric heating components. Non-electric sample temperature control has been realized for a scanning SQUID microscope by mixing liquid helium and helium gas at room temperature.[22] However, such a setup typically involves many metal parts and piezo-motors. Thus, it would need to be redesigned to achieve an ultra-low magnetic background.

In this work, we present the realization of a novel experimental setup,[23] which enables temperature-dependent field measurements of magnetically ordered materials in an ultra-low magnetic background of less than 150 nT. In order to adjust the sample temperature without electric heating, an appropriate mixture of cold liquid helium and warm helium gas is moved past the sample. The setup materials mainly consist of very low remanence materials, such as PolyEther Ether Ketone (PEEK) and PolyVinyl Chloride (PVC). Furthermore, the sample movement and positional encoding are pneumatic and optical, respectively.

II. DESCRIPTION OF EXPERIMENTAL SETUP

The measurement principle is based on determining the temperature and angular dependence of exterior magnetic fields for samples in an ultra-low magnetic background. This is realized with a custom-built continuous Variable Temperature Magnetometer Insert (VTMI), as schematically depicted in Fig. 2. Liquid and gaseous helium enter and then flow downward into the VTMI. At the bottom, the mixture enters the sample tube where it flows upward and thermalizes the sample. A small thermometer mounted to the end of a small hollow temperature holder is placed centrally above the sample to measure the temperature of the upwardly flowing helium mixture. The sample tube can be moved to rotate the sample in front of a SQUID magnetometer. In order to perform such measurements, in practice, the VTMI fulfills additional design conditions.

- The SQUID magnetometer is based on the superconductivity of niobium (Nb) and is operated at liquid helium temperature. A superconducting pick-up coil consisting of niobium titanium (NbTi) is placed in close proximity to the sample, while an isolation vacuum surrounding the sample chamber is realized, which requires a further layer of material. Thus, an additional short transfer tube to bring the liquid helium into the sample chamber is needed.
- Only low remanence magnetic materials should be used for the construction, especially regarding moving parts and all parts near the sample and SQUID to avoid magnetic background.
- To enable rotation and vertical movement of the sample holder tube, a rotation-compatible solution for extracting the helium mixture past the sample is called for, along with seals, which enable these movements while remaining gas-tight. Further tight seals are needed to ensure that the thermometer tube remains fixed during the measurements.

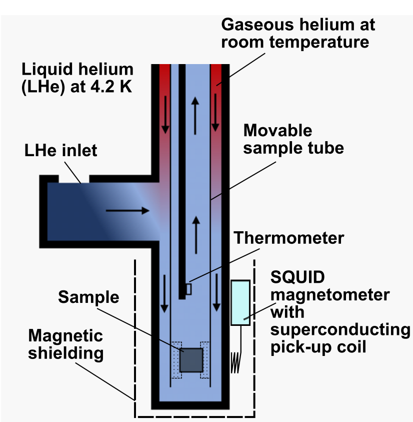

FIG. 2. Schematic measurement principle of the VTMI.

The design of the VTMI is depicted in Fig. 3 and was realized as follows. Double-walled tubes, made of PEEK in its lower part and standard commercial stainless steel of type X5CrNi18-10 in its top part, are glued with STYCAST® 2850 FT[24] to a PEEK needle valve housing. The volume enclosed by the double-walled tubes is evacuated to ensure an isolating vacuum using an exterior turbovacuum pump. The needle valve housing supplies liquid helium from the GFC via a small built-in tunnel between the inner tube and the hole for the needle valve while preserving the isolating vacuum. A gas valve controls the supply of exterior compressed helium gas at room temperature.

A carbon fiber sample holder tube is held via several vacuum seals at its top. Its bottom part is glued with epoxy to a ring-shaped, threaded PEEK connector, which is screwed to a hollow, threaded PEEK counterpart. The latter is glued with epoxy to a plastic straw, in which the sample is fixed with helium-permeable holding pads, manually custom-made from plastic drinking straw material to fit the sample shape. The threaded PEEK parts simplify sample changing. The top part of the sample holder tube features two small holes and is located in ambient room temperature, where it connects to an exhaust valve, such that the liquid and gaseous helium mixture can flow past the sample. A hollow rod within the sample holder tube holds a small Cernox® thermometer (CX-1050-BC-HT)[25] in the gas flow centrally above the sample. Several vacuum seals ensure that the sample holder tube can rotate, while the thermometer rod remains fixed and centered using a centering piece such that helium gas can flow toward the exhaust valve. The thermometer wires (phosphor bronze/copper leads in the cryogenic/room temperature

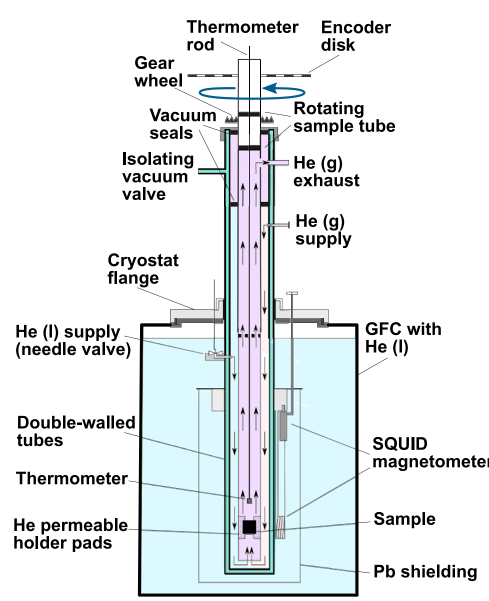

FIG. 3. Schematic view of the realized VTMI[23] placed in a GFC.

region) run through the hollow thermometer rod to electronics at room temperature.

The sample movement is provided by an ultra-low field drive, which is realized as a three cylinder pneumatic engine using commercially available LEGO® and custom-built plastic parts, as depicted in Fig. 4. While the pneumatic engine itself runs at about 120 rpm at a pressure of ≈ 1.5 bars, it is geared down several times to increase the torque, which is needed for rotating the sample holder tube between the seals. The resulting rotation speed of the sample holder is ≈ 0.5 rpm. The sample position is determined using a custom-built optical system, which is realized as a three-channel quadrature encoder consisting of SensoPart® FL 70 light sensors,[26] optical fiber cables, an optical fork barrier, and a plastic encoder disk. The current prototype has an angular sample resolution of 5°.

A PVC mounting supports the SQUID magnetometer and an optional superconducting lead (Pb) shielding. These components and the needle valve piece of the double-walled tubes are completely immersed in the liquid helium of the GFC and attached to the bottom part of the double-walled tube. The SQUID magnetometer is based on a PTB C6XXL1 single-stage current sensor.[27] Due to the Nb materials used in the chip, the sensor is operated at the very stable temperature of LHe at 4.2 K. The control and readout of the sensor were done using Magnicon GmbH XXF-1 electronics.[28] The output voltage of the SQUID electronics was read out with a Keithley® 2010 multimeter[29] at a readout rate of 5 Hz. The current sensor is connected to a superconducting pick-up coil, which consists of 11 turns of NbTi wire (diam. 0.102 mm) wrapped around a PEEK tube of 10.5 mm diameter. The coil had a calculated inductance of ~900 nH. The leads to the coil were carefully twisted to avoid parasitic inductance, which was estimated to be ~ 50 nH as the leads had an approximate length of 0.1 m. The pick-up coil geometry was analogous to that used for a different calibrated SQUID system,[19] and the inductance of the pick-up coil was matched to the SQUID sensor used. The resulting filling factor proved to be appropriate for subsequent test measurements; see Sec. III. In our setup, the minimum distance from the sample to the pick-up coils is 12.5 mm, which is determined by the diameter of the sample chamber and the double walled-vacuum pipes. The filling factor of the pick-up coils decisively depends on this distance, the field of the sample, and the pick-up coil diameter. If the filling factor needs to be improved by optimizing the coil geometry, one could, e.g., use finite-element simulation software. First, the vector potential of the sample material's unit cell is calculated and used as software input along with the sample volume geometry to calculate the magnetic field. Second, the pick-up coil geometry is parametrically varied to simulate the filling factor while the sample rotates.

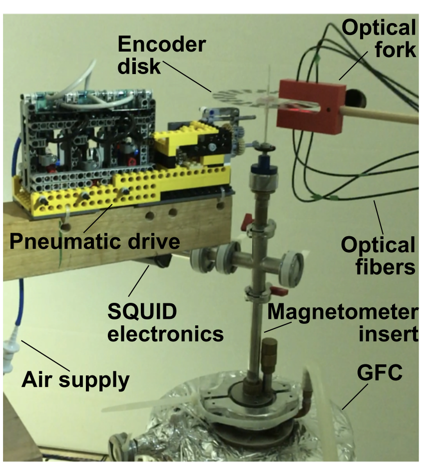

FIG. 4. The non-electric sample movement drive and optical position encoder in operation with a liquid helium temperature magnetometer insert.[19] (Multimedia available online).

The complete measurement setup consists of electronics and vacuum pumps outside of a magnetic shielding, which contains a GFC with the custom-built VTMI, as depicted in the supplementary material.

III. OPERATING PRINCIPLE

Before operation, the sample is placed within the sample tube in front of the SQUID magnetometer. While still at room temperature, an isolating vacuum of ~10^{-4} mbar is pumped. The sample holder tube is carefully flooded with gaseous helium at a slight differential pressure of around 10 mbar. The VTMI is cooled down by careful lowering into the helium-filled GFC and by fixing it at the cryostat flange such that the liquid helium level is well above the needle valve housing. The needle valve is opened to allow liquid helium to enter from the GFC into the sample chamber. To set the temperature, room-temperature helium gas is led into the sample chamber, and when the exhaust valve is kept open, the helium mixture flows through the outer sample holder tube and the sample is thermalized. To achieve a low consumption of helium and to avoid unwanted vibrations, which could cause slight shaking of the sample, the setup is operated at minimal flows. For temperatures above the boiling temperature of liquid helium at normal pressure, i.e., >4.2 K, gas flows corresponding to between 10 and 25 mbar of differential pressure in the exhaust pipe are used.

During operation, the temperature must be set manually by adjusting the helium gas valve and liquid helium needle valve. If the temperature at the sample location is intended to decline, the needle valve may be opened a little further or one may gradually close the helium gas valve. To increase the temperature, one proceeds vice versa. The settings of the valves should result in a pressure of the mixture flow within the verified range corresponding to 10–25 mbar. Comparably high temperatures >100 K can necessitate the complete closing of the needle valve. To reach temperatures below the boiling point of liquid helium at normal pressure, the setup makes use of the decreasing boiling temperature at diminishing pressure. Therefore, the sample chamber must be filled with some liquid helium, and then, the needle valve must be closed further, partially or completely. The connected rotary vane vacuum pump lowers the sample chamber pressure such that sample temperatures as low as 1.5 K can be reached.

During development, tests of the variable temperature insert under realistic measurement conditions, with a sample dummy and two thermometers (one attached to the sample dummy and one at standard position), were performed as depicted in the supplementary material. The temperature difference was lower than

1 K. The *in situ* temperature range proved to be 1.5–65 K with a temperature stability ±2 K of several minutes. The helium consumption was ~1.5 l/h, which allows for over 120 rotations of the sample within one run, corresponding to approximately four hours of measurement time for the 8 l GFC that we used.

The magnetometer component was tested using a 3D-printed magnetic nanomaterial phantom reference sample[30] with designed magnetic dipole response and very low remanence. When the sample was rotated, the SQUID output voltage showed the expected periodicity of 360°, as depicted in the supplementary material. The pick-up coil detects the radial field of the sample and was placed and designed such that the filling factor from the thermometer magnetic field was minimized. For test purposes, the thermometer readout instrument was turned on and off several times to see if this impacted

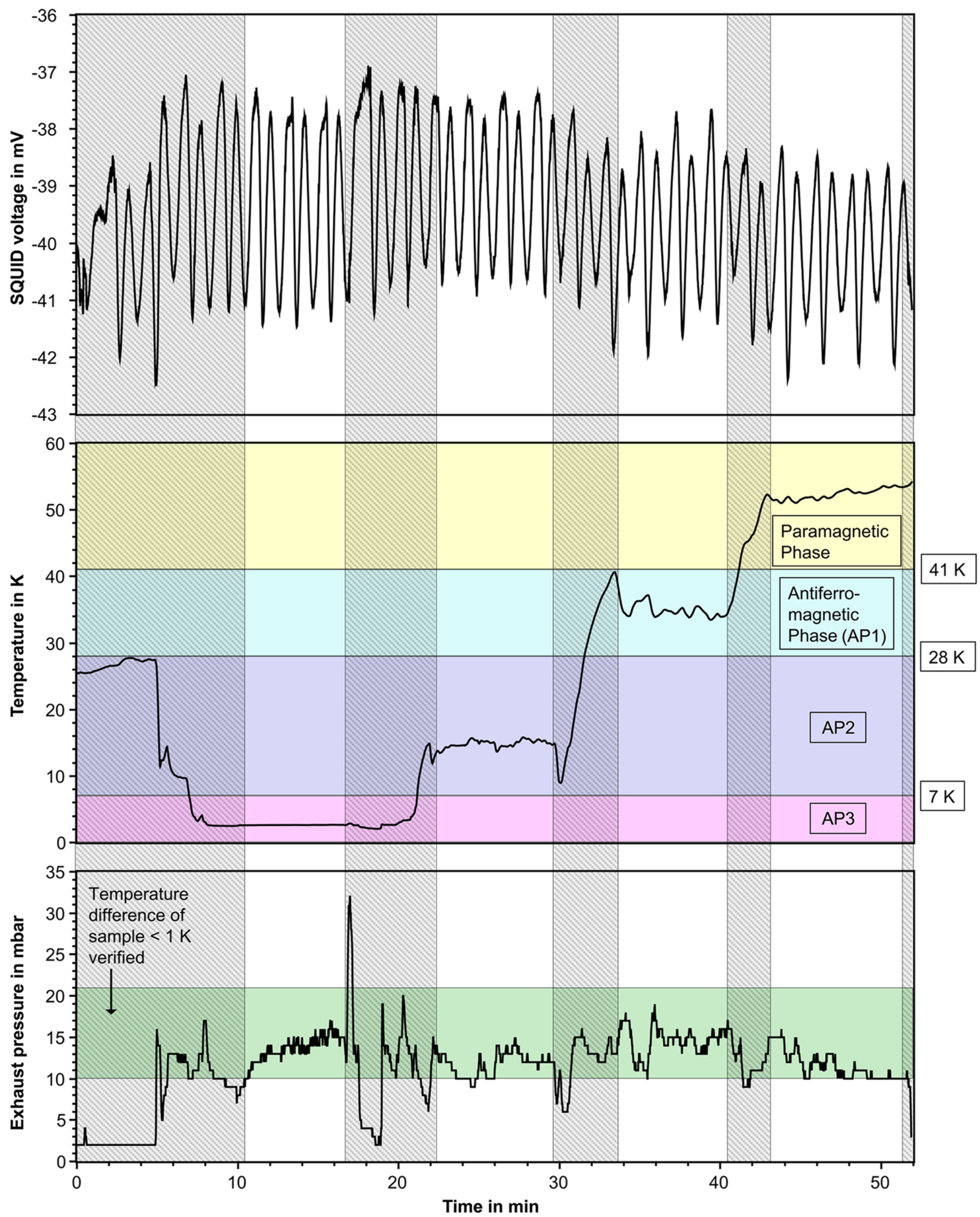

FIG. 5. Raw data plot of a test measurement using the novel setup: a $TbMnO_3$ sample was rotated at ≈ 0.5 rpm. The output SQUID voltage (top), thermometer temperature (middle), and exhaust pressure (bottom) are shown, with transitions and stable regions depicted as **shaded** and **transparent**, respectively.

the magnetic signal detected by the SQUID. While a small peak in magnetic signal could be seen when the thermometer was powered on, there was no visible difference between when the thermometer was on and off. Thus, for the purposes of our test measurement, the magnetic impact of the thermometer was negligible.

When the realized setup was placed in the magnetically shielded room BMSR-2 at PTB Berlin, the magnetic background field *in situ* was measured to be significantly less than 150 nT using hand-held fluxgate devices. The main magnetic contribution came from a remanent steel part in the needle valve, which, in principle, could be replaced with a PEEK version to allow for <10 nT *in situ* magnetic background.

IV. PROTOTYPICAL MEASUREMENT

In order to demonstrate the sensitivity of our setup, we performed temperature-dependent measurements on spin-spiral multiferroic $TbMnO_3$.[31] The material exhibits different magnetic phase transitions at cryogenic temperature, going from paramagnetic (PM) to sinusoidal (AFM1) to cycloidal (AFM2) to Tb^{3+} induced (AFM3) antiferromagnetic order as explained elsewhere.[4,12] Most important for this work are that the magnetic order and transition temperatures are well-known and it is established that $TbMnO_3$ displays compensated spin structures that allow only for weak higher-order contributions, whereas magnetic dipole contributions are forbidden by symmetry in the antiferromagnetic phases, with the temperature intervals of interest[4] PM > T_N = 41 K > AFM1 > T_C = 28 K > AFM2 > T_A = 7 K > AFM3.

Figure 5 represents a temperature-dependent measurement gained on a $TbMnO_3$ single crystal cube with side length ≈ 5 mm. The recorded output SQUID voltage, thermometer temperature, and the exhaust pressure are plotted over the measurement time, which was 52 min. At the start, while rotating the sample using the pneumatic drive, the liquid helium needle valve was opened and the valve for room-temperature helium gas was gradually closed. This caused the temperature to reach a stable 1.5 K, i.e., the AFM3 state of the sample, for 6 min. By closing the needle valve and opening the helium gas valve appropriately, the AFM2, AFM1, and, finally, the PM state of the sample were measured. A periodicity of 180°, i.e., a necessary condition for a quadrupolar field, could be observed for the net signal of the $TbMnO_3$ sample in all antiferromagnetic phases.

The intended functionality of the developed setup was successfully demonstrated. Both the classically known material[14–17] Cr_2O_3 as well as antiferromagnetic $TbMnO_3$ seem to have dominant quadrupolar components in their macroscopic magnetic fields. In order to make comparisons with the benchmark micromagnetic data from neutron scattering,[11,12] further measurements and a full evaluation are needed. This will be addressed in a future work.

V. SUMMARY

A novel setup designed for measuring ultra-small magnetic fields was presented. It is readily applicable to measure weak magnetic remanence of a wide range of solid state materials, including spin-spiral multiferroics,[32] spin ices,[33] and 3D printed nanomaterials,[30] which are used as phantoms in magnetic resonance imaging research.[34] Compared to other setups reported in the literature and commercial SQUID systems, the apparatus features several advantages. The sample movement and thermalization are entirely composed of non-metallic and non-electric components, which greatly reduces magnetic interactions with the sample along with customized state-of-the-art SQUID magnetometry. The setup performed excellently in a controlled, magnetically shielded room. The realized prototype can measure the magnetic field of small (diameters ~1–7 mm) very weakly remanent (~0.1 pT at sample surface) samples in the temperature range 1.5–65 K with an *in situ* background field well below 150 nT, giving new opportunities for the study of complex low-remanent materials with otherwise hard-to-measure magnetic properties.

SUPPLEMENTARY MATERIAL

For benefit of the reader, we have supplemented a movie showing the pneumatic sample movement and optical encoding. To clarify, the multipolar expansion of the vector potential was added. We also provide a detailed overview of the full experimental setup and a photograph of its realization. Furthermore, there are plots showing the thermometry and the SQUID output voltage of a dipolar phantom sample measurement along with a comparison to the $TbMnO_3$ measurement of Fig. 5.

ACKNOWLEDGMENTS

The technical support of Martin Petsche at HZB, Lars Schikowski at PTB, Monique Klemm, and Sassan AliValiollahi at Magnicon GmbH is gratefully acknowledged. The setup was tested at BMSR-2 within the Deutsche Forschungsgemeinschaft core facility *Metrology for Ultra-Low Magnetic Fields* with the generous help of Rainer Körber, Allard Schnabel, and Jens Voigt. The authors thank Tsuyoshi Kimura for providing the $TbMnO_3$ single crystal for our experiments. The authors further thank Niclas Scholz (manufacturing), Dirk Gutkelch (development), and Norbert Löwa (research) of the B-smart Lab at PTB for the support with additive manufacturing concerning a 3D-printed magnetic nanomaterial phantom sample that was kindly provided to us. D.M. acknowledges funding from the Research Council of Norway, Project No. 263228, and support through its Centres of Excellence funding scheme, Project No. 262633, "QuSpin," and also acknowledges NTNU for support via the Onsager Fellowship Program and the Outstanding Academic Fellows Program.

AUTHOR DECLARATIONS

Conflict of Interest

The authors have no conflicts to disclose.

Author Contributions

Michael Paulsen: Conceptualization (lead); Data curation (lead); Formal analysis (lead); Investigation (lead); Methodology (supporting); Project administration (supporting); Resources (supporting); Software (lead); Supervision (lead); Validation (lead); Visualization (lead); Writing – original draft (lead); Writing – review & editing (supporting). **Julian Lindner**: Conceptualization (equal); Data curation (equal); Formal analysis (equal); Investigation (equal); Methodology (equal); Validation (equal); Visualization (equal); Writing – review & editing (supporting). **Bastian Klemke**: Conceptualization (lead); Methodology (lead); Resources (equal); Supervision (supporting). **Jörn Beyer**: Conceptualization (supporting); Funding acquisition (supporting); Investigation (supporting); Project administration (supporting); Resources (equal); Supervision (equal); Validation (equal). **Michael Fechner**: Conceptualization (equal); Formal analysis (lead); Methodology (equal); Software (equal); Supervision (equal); Validation (equal); Visualization (equal). **Dennis Meier**: Conceptualization (equal); Funding acquisition (lead); Investigation (equal); Methodology (equal); Project administration (equal); Resources (equal); Supervision (lead); Writing – original draft (equal); Writing – review & editing (lead). **Klaus Kiefer**: Conceptualization (equal); Funding acquisition (equal); Investigation (supporting); Methodology (supporting); Project administration (lead); Resources (lead); Supervision (equal).

DATA AVAILABILITY

The data that support the findings of this study are available from the corresponding author upon reasonable request.

REFERENCES

[1] F. Pobell, *Matter and Methods at Low Temperatures* (Springer Science & Business Media, 2007).

[2] J. Vrba, "Magnetoencephalography: The art of finding a needle in a haystack," Physica C **368**, 1–9 (2002).

[3] T. Goto, T. Kimura, G. Lawes, A. Ramirez, and Y. Tokura, "Ferroelectricity and giant magnetocapacitance in perovskite rare-earth manganites," Phys. Rev. Lett. **92**, 257201 (2004).

[4] T. Kimura, "Spiral magnets as magnetoelectrics," Annu. Rev. Mater. Res. **37**, 387–413 (2007).

[5] A. Arkenbout, T. Palstra, T. Siegrist, and T. Kimura, "Ferroelectricity in the cycloidal spiral magnetic phase of $MnWO_4$," Phys. Rev. B **74**, 184431 (2006).

[6] J. White, T. Honda, K. Kimura, T. Kimura, C. Niedermayer, O. Zaharko, A. Poole, B. Roessli, and M. Kenzelmann, "Coupling of magnetic and ferroelectric hysteresis by a multicomponent magnetic structure in Mn_2GeO_4," Phys. Rev. Lett. **108**, 077204 (2012).

[7] S. Mühlbauer, B. Binz, F. Jonietz, C. Pfleiderer, A. Rosch, A. Neubauer, R. Georgii, and P. Böni, "Skyrmion lattice in a chiral magnet," Science **323**, 915–919 (2009).

[8] W. Münzer, A. Neubauer, T. Adams, S. Mühlbauer, C. Franz, F. Jonietz, R. Georgii, P. Böni, B. Pedersen, M. Schmidt, A. Rosch, and C. Pfleiderer, "Skyrmion lattice in the doped semiconductor $Fe_{1-x}Co_xSi$," Phys. Rev. B **81**, 041203 (2010).

[9] K. Matsuhira, Y. Hinatsu, and T. Sakakibara, "Novel dynamical magnetic properties in the spin ice compound $Dy_2Ti_2O_7$," J. Phys.: Condens. Matter **13**, L737 (2001).

[10] T. Jungwirth, X. Marti, P. Wadley, and J. Wunderlich, "Antiferromagnetic spintronics," Nat. Nanotechnol. **11**, 231–241 (2016).

[11] B. N. Brockhouse, "Antiferromagnetic structure in Cr_2O_3," J. Chem. Phys. **21**, 961–962 (1953).

[12] M. Kenzelmann, A. B. Harris, S. Jonas, C. Broholm, J. Schefer, S. Kim, C. Zhang, S.-W. Cheong, O. P. Vajk, and J. W. Lynn, "Magnetic inversion symmetry breaking and ferroelectricity in $TbMnO_3$," Phys. Rev. Lett. **95**, 087206 (2005).

[13] M. Buchner, K. Höfler, B. Henne, V. Ney, and A. Ney, "Tutorial: Basic principles, limits of detection, and pitfalls of highly sensitive SQUID magnetometry for nanomagnetism and spintronics," J. Appl. Phys. **124**, 161101 (2018).

[14] I. Dzyaloshinskii, "External magnetic fields of antiferromagnets," Solid State Commun. **82**, 579–580 (1992).

[15] D. Astrov and N. Ermakov, "Quadrupole magnetic field of magnetoelectric Cr_2O_3," Sov. J. Exp. Theor. Phys. Lett. **59**, 297 (1994).

[16] D. Astrov, N. Ermakov, A. Borovik-Romanov, E. Kolevatov, and V. Nizhankovskii, "External quadrupole magnetic field of antiferromagnetic Cr_2O_3," J. Exp. Theor. Phys. Lett. **63**, 745–751 (1996).

[17] A. Borovik-Romanov and V. Nizhankovskii, "Quadrupolar magnetic field outside antiferromagnetic Cr_2O_3," Acta Phys. Pol. A **92**, 371–374 (1997).

[18] Quantum Design, Inc., "MPMS 3 platform measurement options: Ultra-low field (ULF) and rotator," 2023, https://www.qdusa.com/siteDocs/productBrochures/1500-103.pdf, Online; accessed 10 May 2023.

[19] M. Paulsen, K. Kiefer, D. Meier, M. Fechner, B. Klemke, M. Petsche, and H. Lucht, "Device for determining small magnetic fields with at least one SQUID sensor," (2019).

[20] S. Knappe-Grueneberg, A. Schnabel, G. Wuebbeler, and M. Burghoff, "Influence of demagnetization coil configuration on residual field in an extremely magnetically shielded room: Model and measurements," J. Appl. Phys. **103**, 07E925 (2008).

[21] Z. Sun, P. Fierlinger, J. Han, L. Li, T. Liu, A. Schnabel, S. Stuiber, and J. Voigt, "Limits of low magnetic field environments in magnetic shields," IEEE Trans. Ind. Electron. **68**, 5385–5395 (2020).

[22] A. Lõhmus, A. Tzalenchuk, V. Korrovits, Z. Ivanov, R. Lõhmus, M. Lobjakas, A. Heinloo, S. Pehrson, and T. Claesson, "Non-magnetic heating for temperature control in scanning SQUID microscope," Physica B **284–288**, 2113–2114 (2000).

[23] J. Lindner, M. Paulsen, K. Kiefer, D. Meier, M. Fechner, B. Klemke, M. Petsche, and L. Schikowski, "Vorrichtung zur variablen temperatureinstellung in einem durchflusskryostaten," Patent Application DE102020123664A1, Granted 23 August 2022.

[24] Emerson & Cuming, "STYCAST 2850 FT, data sheet," 2023, https://www.paisleyproducts.com/content/files/content/tds/AVEM50FT_tds_1_1_2015.pdf, Online; accessed 10 May 2023.

[25] Lake Shore Cryotronics, Inc., "Cernox RTDs, CX-1050," 2023, https://www.lakeshore.com/docs/default-source/product-downloads/catalog/lstc_cernox_l./pdf?sfvrsn=41b96c23_6, Online; accessed 10 May 2023.

[26] SensoPart Industriesensorik GmbH, "Optical sensor FL 70," 2023, https://www.sensopart.com/en/products/details/567-71000/, Online; accessed 10 May 2023.

[27] D. Drung, C. Assmann, J. Beyer, A. Kirste, M. Peters, F. Ruede, and T. Schurig, "Highly sensitive and easy-to-use SQUID sensors," IEEE Trans. Appl. Supercond. **17**, 699–704 (2007).

[28] Magnicon GmbH, "XXF-1 SQUID electronics, data sheet," 2023, https://www.magnicon.com/fileadmin/user_upload/downloads/datasheets/Magnicon_XXF-1.pdf, Online; accessed 10 May 2023.

[29] Tektronix, Inc., "Keithley 2010 multimeter, data sheet," 2023, https://download.tek.com/document/SPEC-2010E_July_2015.pdf, Online; accessed 10 May 2023.

[30] N. Löwa, J.-M. Fabert, D. Gutkelch, H. Paysen, O. Kosch, and F. Wiekhorst, "3D-printing of novel magnetic composites based on magnetic nanoparticles and photopolymers," J. Magn. Magn. Mater. **469**, 456–460 (2019).

[31] T. Kimura, T. Goto, H. Shintani, K. Ishizaka, T.-h. Arima, and Y. Tokura, "Magnetic control of ferroelectric polarization," Nature **426**, 55–58 (2003).

[32] M. M. Vopson, "Fundamentals of multiferroic materials and their possible applications," Crit. Rev. Solid State Mater. Sci. **40**, 223–250 (2015).

[33] M. J. Gingras, "Spin ice," in *Introduction to Frustrated Magnetism* (Springer, 2011), pp. 293–329.

[34] M. A. A. Arenas, D. Gutkelch, O. Kosch, R. Brühl, F. Wiekhorst, and N. Löwa, "Development of phantoms for multimodal magnetic resonance imaging and magnetic particle imaging," Polymers **14**, 3925 (2022).